The Underwater Swimming Manipulator—A Bioinspired Solution for Subsea Operations

Jørgen Sverdrup-Thygeson, Eleni Kelasidi, Kristin Y. Pettersen, *Fellow, IEEE*, and Jan Tommy Gravdahl

***Abstract*—Underwater vehicles have carried out subsea operations for many decades, and since the 1980s, remotely operated vehicles (ROVs) have been essential for the development and maintenance of subsea installations. As the technology has progressed, various types of vehicles have been developed to perform subsea inspection, maintenance, and repair (IMR) operations, including conventional work class ROVs, inspection class ROVs, autonomous underwater vehicles (AUVs), and, more recently, intervention AUVs. The underwater swimming manipulator (USM), presented in this paper, is an innovative bioinspired addition to the family of underwater robotic vehicles. The overall vision of the USM is to provide a significant impact on how to perform inspection and light intervention tasks. In this paper, we discuss the most important applications for the USM and the main challenges related to modeling, guidance, and control of this innovative vehicle. We provide a detailed description of the concept of the USM, together with a proposed generic motion control framework. A kinematic and dynamic model of the USM is derived for the purpose of designing control algorithms, and selected task-based control approaches are presented, based on inverse kinematic control. We also present the development of a simulation environment, a simulation model of the USM, and provide simulations to support the use of USMs for subsea IMR operations.**

***Index Terms*—Manipulators, motion control, robot control, robot kinematics, robot motion, unmanned underwater vehicles.**

I. Introduction

FOR several decades, the traditional remotely operated vehicle (ROV) has been the workhorse used for any kind of subsea operations. Currently, the industry is facing an important shift toward more economical and more efficient operations on subsea installations, and the use of conventional ROVs is, in many situations, considered too expensive. Ageing subsea infrastructure calls for more preventive maintenance, and the needs for routine inspections increase as the number of new subsea installations continue to grow. Consequently, the industry has recognized the need for lighter, less costly, and more specialized vehicles that can perform various autonomous and semiautonomous tasks at subsea oil and gas installations [1]. In particular, lightweight autonomous underwater vehicles (AUVs) with hovering, precise maneuvering, and even light intervention capabilities experience increased attention [2]–[5].

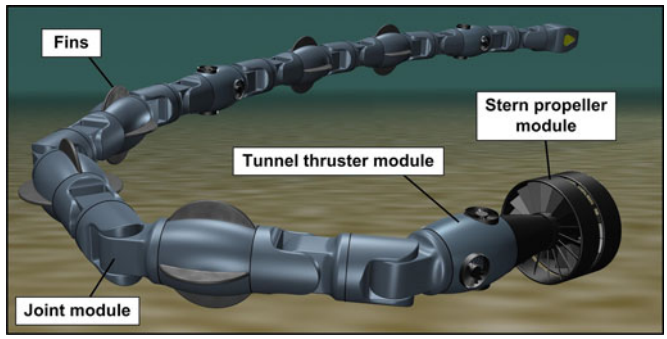

Fig. 1. Generic illustration of a USM.

In this paper, we present the novel concept of an underwater swimming manipulator (USM), which is an innovative bioinspired AUV that to a large extent can replace or assist ROVs with expensive support vessels, for carrying out inspections and light intervention tasks. The USM is a snake-like multibody robotic mechanism consisting of serially connected links, equipped with longitudinal thrusters and tunnel thrusters along the body. A generic illustration is shown in Fig. 1.

To realize operational USMs for inspection and light intervention tasks, several theoretical problems such as modeling, guidance, and control should be addressed. In this paper, we present a generic motion control framework for the USM, with particular focus on kinematic control, dynamic control, and thrust allocation for the USM. Each part of the framework is thoroughly discussed, and solutions are proposed and simulated for each subsystem, to show the applicability of the motion control framework for guidance and control of the USM. We also discuss possible applications and the main advantages of using a USM for subsea inspection, maintenance, and repair (IMR) operations, together with a comparison between the USM and existing solutions. Preliminary results toward this have been presented in [6]–[8]. In this paper, we extend these results and provide a unified presentation of the concept of the USM, kinematic and dynamic modeling, and control strategies to provide a clear and consistent overview of the current status of this research and to act as a foundation for future work.

Manuscript received January 29, 2017; revised August 9, 2017; accepted October 23, 2017. Date of publication November 28, 2017; date of current version April 12, 2018. This work was supported in part by the Research Council of Norway through the Centres of Excellence Funding Scheme under Project 223254 NTNU AMOS, and in part by VISTA, a basic research program in collaboration between The Norwegian Academy of Science and Letters, and Statoil. *(Corresponding author: Jørgen Sverdrup-Thygeson.)*

Associate Editor: T. Maki.

J. Sverdrup-Thygeson, E. Kelasidi, and K. Y. Pettersen are with the Centre for Autonomous Marine Operations and Systems, Department of Engineering Cybernetics, Norwegian University of Science and Technology, Trondheim 7491, Norway (e-mail: Jorgen.Sverdrup-Thygeson@ntnu.no; Eleni.Kelasidi@ntnu.no; Kristin.Y.Pettersen@ntnu.no).

J. T. Gravdahl is with the Department of Engineering Cybernetics, Norwegian University of Science and Technology, Trondheim, 7491, Norway (e-mail: Tommy.Gravdahl@ntnu.no).

Digital Object Identifier 10.1109/JOE.2017.2768108

In the modeling part of this paper, the kinematic model is extended by deriving expressions for the geometric link Jacobians, using a method inspired by From *et al.* [9]. This modeling approach is well suited for USMs, since it provides compact matrix expressions, easy implementation, and a flexibility that accommodates an arbitrary number of links, with variable link length, and free choice of the base of the USM. The expressions are also valid if the USM includes prismatic joints, e.g., an extendable gripper tool attached to the front link. The geometric Jacobians are then utilized to derive the state-dependent rigid body inertia matrix and the state-dependent thruster configuration matrix (TCM) of the USM in 3-D. Note that the derivation of the TCM is essential, as it is a prerequisite for successful implementation of any dynamic control approach. Finding the TCM for a USM is more challenging than for typical underwater vehicles, since the position and orientation of the thrusters relative to the base of the USM depend on the joint angles.

In the control part of this paper, we utilize the kinematic model to study motion coordination of the joints and the base of the USM, using task based control methods, and we present the fundamental differences between inverse kinematic control of a USM and a typical underwater vehicle equipped with a robotic arm. Previous research on redundant ground-based robots and underwater vehicle-manipulator systems (UVMSs) has revealed a number of different solutions for redundancy resolution, considering various performance criteria. Most of the proposed ideas are based on the first-order or second-order inverse kinematics of the robot manipulators. The manipulability criteria is considered in, e.g., [10] for a ground-based robot, where the trajectory of the mobile base is calculated to maximize the manipulability index of the two-link manipulator arm, and in [11] for a UVMS. In [12], set-based tasks are used to keep the manipulability index above a specified minimum value. Obstacle avoidance for redundant manipulators is investigated in, e.g., [13], and drag optimization is considered in [14]. Kinematic control of a UVMS using the task priority approach has been extensively studied in [15]–[19] among others. In this paper, we investigate the use of the singularity robust multiple task priority (SRMTP) method [20]–[22] for null-space-based kinematic control of the USM. A preliminary discussion of kinematic control of a USM was given in [7] and [8]. Here, we extend these results by providing a singularity free quaternion formulation for the primary end-effector task, and we discuss how to apply the SRMTP method to fulfill the secondary control objectives for the USM.

A large number of methods have been proposed in the literature for dynamic control of underwater single-body vehicles and underwater robotic vehicles; see, e.g., [23] and [24] and references therein. In this paper, we propose to use a standard feedback linearization method for dynamic control of the base of the USM. The output from the dynamic controller is fed to the thrust allocation module, which is in charge of optimally distributing the thruster forces. A number of different methods for optimal thrust allocation of marine vehicles have been proposed in, e.g., [25]–[29] for surface vessels, and in [30] and [31] for underwater vehicles. A recent survey on control allocation methods, in general, is given in [32]. In this paper, we propose a thrust allocation method that takes near-singular thruster configurations into account, since the TCM can become ill-conditioned when the position and orientation of the thrusters relative to the USM base change when moving the joints.

Furthermore, we propose to divide the operation of the USM into two distinct modes, namely, transport mode and work mode. In particular, we provide a thorough discussion of each mode and propose control strategies for both modes, thus extending the initial presentation in [7]. In [8], a preliminary 3-D simulation model for an underactuated USM was implemented in the multibody simulation tool Vortex [33], and a computer simulation environment was set up to allow testing of various control algorithms. In this paper, we present a new and improved simulation model of a fully actuated USM, and thoroughly discuss the process of developing this 3-D model. The new model is then used, for the first time, to perform 3-D simulations in Vortex using the inverse kinematics algorithm combined with the dynamic control law for the USM base motion and the thrust allocation method. This provides more realistic simulation results supporting the applicability of the motion control framework.

The remainder of this paper is structured as follows. In Section II, the application of the USM for subsea IMR operations is discussed and compared to existing technology. The development of a mathematical model of the USM for control purposes is presented in Section III, while the proposed motion control framework and the various subsystems are thoroughly discussed in Section IV. Section V presents the two modes of operation for the USM, and finally, Section VI provides the combined kinematic and dynamic simulations, supporting the applicability of the motion control framework. Conclusions and future directions for the ongoing research on USMs are presented in Section VII.

II. Applications and Existing Technology

For decades, the standard way of performing subsea IMR operations has been by using conventional work class ROVs. Gradually, AUVs and smaller inspection class ROVs have taken over some of the tasks, mainly those involving inspections. In this section, we explain the benefits of the USM and investigate how USMs can contribute to and complement the existing solutions used for subsea IMR operations. We also discuss other suitable applications for the USM. This section complements and extends the discussion on applications and existing technology in [8].

A. Comparison With Existing Technology

Conventional work class ROVs are expensive to operate, as they require the support of a surface vessel, a specialized crew to deploy and operate them, and constant supervision. Further economical losses may be incurred because the time to mobilize and deploy these large ROVs is quite long. On the other hand, work class ROVs can operate in deep waters and are equipped with powerful robotic arms capable of performing heavy intervention tasks. Inspection class ROVs are much smaller, easier to deploy, and cheaper to operate. However, they are not powerful enough to perform heavy intervention, and their robotic arms

TABLE I
COMPARISON OF VARIOUS FEATURES OF USMS, ROVS, AUVS, AND I-AUVS

Feature	USM	Inspection ROV	Small AUV	I-AUV (existing)
Size and weight	Small, lightweight	Small, lightweight	Small, lightweight	Large, heavy
Supervision and control	Supervised autonomy	Manually controlled	Supervised autonomy	Supervised autonomy
Commutable payload	Yes	Yes	No	No
Payload capacity	Medium	Medium	Medium	Large
Collision consequence	Medium	Medium	Medium	Severe
Accessibility	Very good	Good	Good	Restricted by size
Kinematic redundancy of manipulator arm	Very high	Low	–	Intermediate
Intervention capability	Yes	Yes	No	Yes
Tethered	No	Yes	No	No
Drag forces	Low	Low	Low	High

are smaller and less flexible than for work class ROVs. Also, ROVs are, in general, limited by the attached tether.

Some of the issues related to ROVs, such as the need for a supporting surface vessel, constant supervision, and tether control, can be resolved by using AUVs. Most commercially available AUVs are single body torpedo-shaped vehicles that are optimized for geophysical surveys, reconnaissance and surveillance operations, and long duration search and recovery missions. Although some of these AUVs possess hovering capabilities and are able to perform stationary tasks, they are not particularly well suited for subsea IMR operations. In 1997, the French company Cybernetix, Marseille, France, proposed a hybrid AUV/ROV concept, called SWIMMER [34], with the purpose of performing light subsea IMR operations without being attached to a support vessel. The vehicle was developed and technical feasibility was confirmed by sea trials in 2001 [35]. In 2007, Cybernetix initiated a cooperation with Total and Statoil with the aim of developing a commercial version of SWIMMER [36]. This hybrid vehicle is limited by its size and the tether between the ROV and the AUV. The increasing interest for innovative solutions for subsea IMR has also led to the development of smaller AUVs capable of performing subsea inspections, such as the autonomous inspection vehicle developed by Subsea 7 [2], SAAB Seaeye Sabertooth [3], and the Marlin AUV by Lockheed Martin [4]. Note that the currently available AUV solutions can, for the most part, provide inspection capabilities, and that manipulation tasks and operations inside tight and confined areas would require the added flexibility of a robotic arm.

AUVs equipped with one or more robotic arms are commonly referred to as intervention AUVs (I-AUVs) [37]. The I-AUVs developed through the research projects ALIVE [38], SAUVIM [39], and RAUVI/Trident [5], [40]–[42] have demonstrated autonomous intervention capabilities in controlled environments such as pools or harbor areas with small environmental disturbances. In 2016, the hybrid ROV/AUV system H-ROV Ariane was officially presented by the ECA Group and Ifremer [43], [44], making it one of the first commercial AUVs with a robotic arm. ALIVE, SAUVIM, and H-ROV Ariane are large and heavy vehicles, which must be deployed by crane and require a large open space to operate safely. Should a heavy vehicle like this collide with subsea infrastructure, the consequences could be severe.

As pointed out in the previous discussion, it would be beneficial to have a small highly maneuverable and flexible vehicle, which is easy to deploy and operate, and is capable of performing both inspection and light intervention tasks. The USM concept introduced in [6] possesses all of these characteristics and has the potential to overcome the challenges mentioned above. A USM is essentially a fusion of an underwater snake robot (USR) and a small AUV. By using thrusters in combination with the articulated joints, the USM can operate as a floating base manipulator. The thrusters ensure that the USM can operate within a large workspace and also maintain position and orientation while performing an inspection or intervention task. The large number of actively controlled joints endows the USM with very good manipulation properties. The combination of a slender and flexible body with a long reach makes the USM superior in terms of accessibility, and thus, the USM can provide access to confined areas that are difficult to access with other types of underwater vehicles. A modular design allows us to add and remove modules to accommodate different payloads and a varying number of thrusters. The USM also has the ability to swim like a biological eel using joint motion alone. This can be important in case of thruster failures or in particular applications where the use of thrusters is not recommended, e.g., close to the seabed or when silent operation is required. For all the reasons mentioned above, we consider the USM as a complete, versatile, and promising system for light subsea IMR operations. Table I summarizes the most important features for subsea inspection and intervention, and compares the USM to other existing underwater vehicles. Next, we discuss various applications that are well suited for USMs.

B. Applications

As explained in Section II-A, the most important benefits of the USM are associated with access to tight spaces, long reach, and hyperredundant characteristics. Confined spaces and narrow passages can be found in conjunction with subsea installations and marine archaeological sites such as shipwrecks and underwater caves. With a diameter of 15 cm or less, the USM is very well suited for investigation of such sites.

For subsea IMR operations, in particular, the USM can be permanently installed underwater with a docking station to recharge the batteries, transfer collected data, and receive updated commands. As such, the USM can perform both planned

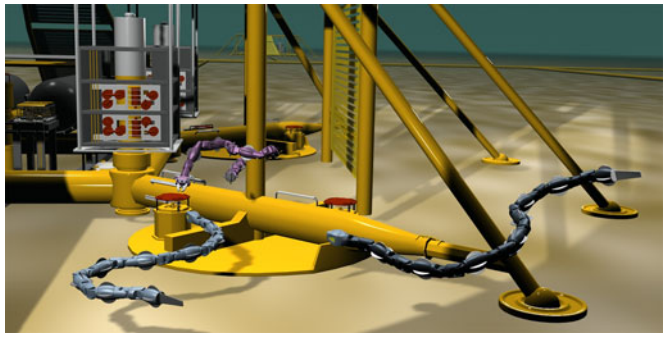

Fig. 2. Inspection and intervention.

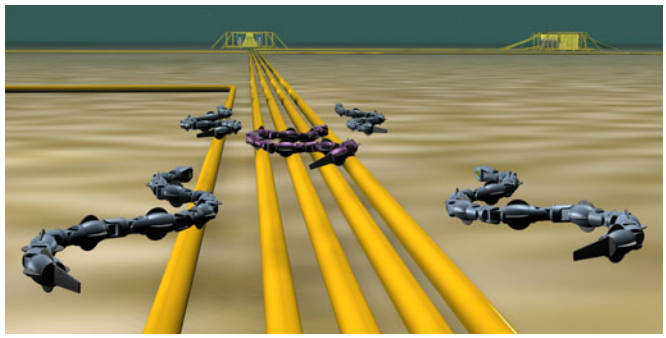

Fig. 3. Pipeline survey.

and on-demand tasks. This is important in terms of preventive maintenance and routine inspections, and it may help to avoid unscheduled shutdowns by reacting instantly when required. The hybrid AUV/ROV SWIMMER, mentioned earlier, was one of the first vehicles to introduce the concept of the field resident AUVs. Similar concepts are also being pursued by Chevron [1] and for the SAAB Seaeye Sabertooth AUV. To the authors' best knowledge, this technology has not yet been commercially realized. An important difference between the USM and the Seaeye AUV is that the USM is much more flexible and maneuverable, and can operate as an underwater robotic arm. The size of the USM is also much smaller, which allows the USM to dock and be launched from a small tube that is easily fitted to existing subsea structures without requiring significant modifications. The long reach and the hyperredundant design enable the USM to attach itself to a suitable handle or grab bar to perform precision tasks such as close-up inspection, cleaning, and opening and closing valves. Besides being used for subsea IMR operations, the USM can also be operated as a conventional AUV to perform harbor and ship hull inspections, installation support, and pipeline surveys. Figs. 2 and 3 illustrate two of the mentioned applications. Although the illustrations depict the use of USRs, the thruster equipped USM is even more appropriate for these tasks.

III. Modeling of the Underwater Swimming Manipulator

In this section, we develop the kinematic and dynamic model of the USM, including derivation of the state-dependent TCM.

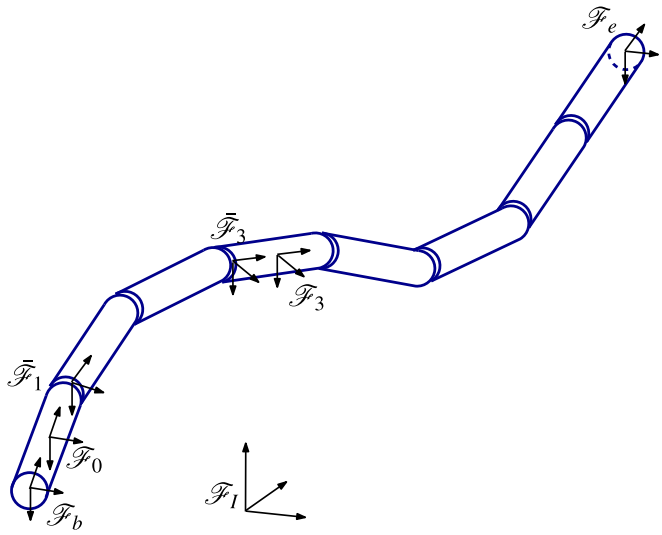

Fig. 4. Reference frames.

First, we extend the kinematic modeling in [7] by deriving the geometric Jacobians associated with each link. Second, we present the dynamic model of the USM and show how to calculate the state-dependent system inertia matrix and the dynamic coupling matrix. Third, we derive the TCM based on the kinematics of the USM.

A. Notation

In this paper, the USM is treated as an underwater robotic manipulator arm with a floating base. The USM consists of $n+1$ links connected by n actuated joints. The links are numbered from the tail forward, indicated by subscripts $i \in [0 \dots n]$. Each link is associated with a link reference frame $\mathscr{F}_i$ attached to the center of mass (CM) of the link. The axes of $\mathscr{F}_i$ coincide with the principle axes of inertia of the link. The base of the USM can, in general, be positioned at any convenient location on the body of the USM. In this paper, the base is chosen to coincide with the back end of link 0, and the term end-effector refers to the front end of link n. The reference frames corresponding to the base and the end-effector are the base frame $\mathscr{F}_b$ and the end-effector frame $\mathscr{F}_e$. The joints have one degree of mobility, and they are numbered with $i \in [1, \dots, n]$, such that the links i and $i-1$ are connected by joint i. The corresponding reference frames $\bar{\mathscr{F}}_i$ are fixed to the center of the joints. Furthermore, the USM is equipped with m thrusters, numbered by $j \in [1, \dots, m]$, including both longitudinal thrusters and tunnel thrusters acting through the links. The thrusters provide both forward propulsion and station-keeping capability by counteracting nonzero buoyancy, ocean currents, and other disturbances. The position and orientation of the thrusters are described by the reference frames $\mathscr{F}_{t_j}$. The frames $\mathscr{F}_{t_j}$ have origins at the points of application of the thruster forces and the *X*-axis points along the thrust vector. Finally, the frame $\mathscr{F}_I$ is an assumed inertial reference frame. The origin and the orientation of each frame are illustrated in Fig. 4.

The USM is an articulated structure that consists of multiple rigid bodies connected to each other, i.e., it is a multibody system. A mathematically convenient and geometrically meaningful way to represent the configuration of each link in the 3-D Euclidean space and the transformations between the links is to use homogeneous transformation matrices. For example, the pose of the frame $\mathscr{F}_b$ with respect to the inertial frame $\mathscr{F}_I$ is given by the homogeneous transformation matrix

$$g_{Ib} = \begin{bmatrix} R_{Ib} & p_{Ib} \\ 0 & 1 \end{bmatrix} \in SE(3) \tag{1}$$

where $R_{Ib} \in SO(3)$ is the rotation matrix describing the orientation of the base frame and $p_{Ib} \in \mathbb{R}^3$ is the vector from the origin of $\mathscr{F}_I$ to the origin of $\mathscr{F}_b$. The transformation in (1) represents a translation by p_{Ib} followed by a rotation given by R_{Ib}. We sometimes use *pose* as a collective term for both position and orientation. An important reason for describing the configuration of the rigid bodies of the USM as elements of the manifold $SE(3)$ is that we avoid singularities in the representation. Such representation singularities will typically appear if the state space is represented in $\mathbb{R}^6$ using Euler angles to describe the orientation.

The body-fixed velocity of the USM is given by

$$\zeta = \begin{bmatrix} V_{Ib}^b \\ \dot{q} \end{bmatrix} \in \mathbb{R}^{6+n}, \quad V_{Ib}^b = \begin{bmatrix} v_{Ib}^b \\ \omega_{Ib}^b \end{bmatrix} \in \mathbb{R}^6 \tag{2}$$

where v_{Ib}^b and ω_{Ib}^b are the body-fixed linear and angular velocities of the base of the USM, respectively, and q is the vector of joint angles. We use the hat operator $\hat{}$ to write angular velocity vectors $\omega \in \mathbb{R}^3$ in skew-symmetric form and also to represent velocity coordinate vectors $V \in \mathbb{R}^6$ as velocity twists

$$\hat{V} = \begin{bmatrix} \hat{\omega} & v \\ 0 & 0 \end{bmatrix}. \tag{3}$$

B. Kinematics

In this section, we will discuss the kinematic redundancy of the USM, and derive the forward and differential kinematics of the mechanism. A robotic mechanism is said to be kinematically redundant if it possesses more independent control inputs than required to satisfy a given task. Thus, the degree of redundancy is defined with respect to a specific task. For the USM, a typical task is to control the end-effector in 6 DOF. A fully actuated USM has enough thrusters to control the base of the USM in 6 DOF, and thus the end-effector task can be satisfied by moving the USM base only. In addition, the USM has n joints that can also be utilized to solve the task. As such, the USM has n redundant degrees of freedom with respect to the 6 DOF end-effector task, i.e., it has a high degree of kinematic redundancy.

Deriving the kinematics of the USM is important for a number of reasons. First, the kinematics are required to resolve the kinematic redundancy of the USM. This will be addressed in Section IV-A where the kinematic control module is described. Second, estimation of the gravitational and buoyancy forces requires knowledge of the orientation of each link. Third, the kinematics are needed to derive the TCM, which is the topic of Section IV-C.

1) Forward Kinematics: The forward kinematics of the USM is given by the transformations between the reference frames defined in Section III-A. The pose of the USM base with respect to the inertial frame is given by (1), while the transformation between two consecutive joints is given by

$$g_{(\overline{i-1})\bar{i}} = \begin{bmatrix} R_{(\overline{i-1})\bar{i}} & p_{(\overline{i-1})\bar{i}} \\ 0 & 1 \end{bmatrix}. \tag{4}$$

Since two consecutive transformations are also a transformation, the pose of the end-effector frame $\mathscr{F}_e$ can be expressed by

$$g_{Ie} = g_{Ib}g_{be} = \begin{bmatrix} R_{Ib} & p_{Ib} \\ 0 & 1 \end{bmatrix} \begin{bmatrix} R_{be} & p_{be} \\ 0 & 1 \end{bmatrix} = \begin{bmatrix} R_{Ie} & p_{Ie} \\ 0 & 1 \end{bmatrix} \tag{5}$$

where g_{be} describes the relative transformation between the base frame $\mathscr{F}_b$ and the end-effector frame $\mathscr{F}_e$. Furthermore, the position and orientation of the reference frames $\bar{\mathscr{F}}_i$ and $\mathscr{F}_i$ attached to the joints of the USM and to the CM of each link, respectively, are given by

$$g_{I\bar{i}} = g_{Ib}g_{b\bar{1}} \cdots g_{(\overline{i-1})\bar{i}} = \begin{bmatrix} R_{I\bar{i}} & p_{I\bar{i}} \\ 0 & 1 \end{bmatrix} \tag{6}$$

$$g_{Ii} = g_{Ib}g_{b1} \cdots g_{(i-1)i} = \begin{bmatrix} R_{Ii} & p_{Ii} \\ 0 & 1 \end{bmatrix}. \tag{7}$$

Finally, the configuration of the thruster frames $\mathscr{F}_{t_j}$ is calculated by $g_{It_j} = g_{Ib}g_{bt_j}$. All these transformation matrices are time varying and the time evolution is investigated next.

2) Differential Kinematics: The differential kinematics describes the relationship between the velocities of different parts of the USM. The body-fixed velocity of the base frame V_{Ib}^b is related to the transformation matrix g_{Ib} by the velocity twist [9]

$$\hat{V}_{Ib}^b = g_{Ib}^{-1}\dot{g}_{Ib} = \begin{bmatrix} \hat{\omega}_{Ib}^b & v_{Ib}^b \\ 0 & 0 \end{bmatrix} \in se(3) \tag{8}$$

where $\hat{\omega}_{Ib}^b$ is the skew-symmetric representation of the angular velocity. The velocity twist of link i with respect to the inertial frame $\mathscr{F}_I$ can then be expressed in frame $\mathscr{F}_i$ by

$$\begin{aligned} \hat{V}_{Ii}^i &= g_{Ii}^{-1}\dot{g}_{Ii} \\ &= (g_{bi}^{-1}g_{Ib}^{-1})(\dot{g}_{Ib}g_{bi} + g_{Ib}\dot{g}_{bi}) \\ &= g_{bi}^{-1}\hat{V}_{Ib}^b g_{bi} + \hat{V}_{bi}^i. \end{aligned} \tag{9}$$

We write the velocity twist in (9) in coordinate form as

$$V_{Ii}^i = Ad_{g_{bi}}^{-1}V_{Ib}^b + V_{bi}^i \tag{10}$$

where $Ad_{g_{bi}}$ is the adjoint map for the transformation g_{bi}. The velocity variable V_{bi}^i represents the relative velocity between the base of the USM and link i. When acting on a coordinate vector V, the adjoint map and its inverse are given by [9]

$$Ad_g = \begin{bmatrix} R & \hat{p}R \\ 0 & R \end{bmatrix}, \quad Ad_g^{-1} = \begin{bmatrix} R^T & -R^T\hat{p} \\ 0 & R^T \end{bmatrix}. \tag{11}$$

In the same way, the body-fixed velocity of the end-effector frame $\mathscr{F}_e$ is found by

$$V_{Ie}^e = Ad_{g_{be}}^{-1} V_{Ib}^b + V_{be}^e. \tag{12}$$

In (10) and (12), the inverse adjoint maps transform the body-fixed velocity vector V_{Ib}^b so that it represents velocities in the link frames $\mathscr{F}_i$ and the end-effector frame $\mathscr{F}_e$, respectively. We write the relative link velocities and end-effector velocity as functions of the joint velocities $\dot{q}$ according to

$$V_{bi}^i = Ad_{g_{bi}}^{-1} J_i \dot{q} \tag{13}$$

$$V_{be}^e = Ad_{g_{be}}^{-1} J_e \dot{q} \tag{14}$$

where the link Jacobians J_i and the end-effector Jacobian J_e are defined by

$$J_i(q) \triangleq \left[Ad_{g_{b\bar{1}}}(q)X_1^1, \ldots, Ad_{g_{b\bar{i}}}(q)X_i^i, 0_{(n-i)\times 6}\right] \tag{15}$$

$$J_e(q) \triangleq \left[Ad_{g_{b\bar{1}}}(q)X_1^1, \ldots, Ad_{g_{b\bar{n}}}(q)X_n^n\right]. \tag{16}$$

For the USM, the joint twist coordinate vectors X_i^i are given by either $X_i^i = [0,0,0,0,0,1]^T$ or $X_i^i = [0,0,0,0,1,0]^T$ depending on whether the joint rotates about the *Z*-axis or the *Y*-axis of frame $\bar{\mathscr{F}}_i$. Finally, by inserting (13) and (14) into (10) and (12), we get

$$V_{Ii}^i = J_{g,i}(q)\zeta, \quad J_{g,i}(q) \triangleq \left[Ad_{g_{bi}}^{-1}, Ad_{g_{bi}}^{-1} J_i\right] \tag{17}$$

$$V_{Ie}^e = J_{g,e}(q)\zeta, \quad J_{g,e}(q) \triangleq \left[Ad_{g_{be}}^{-1}, Ad_{g_{be}}^{-1} J_e\right] \tag{18}$$

where $J_{g,i}$ and $J_{g,e}$ are the geometric Jacobians, which map the base frame and the joint velocities to the linear and angular velocities of each link and the end-effector, respectively. For further theoretical details about this geometric approach, we refer to [9].

C. Equations of Motion

The USM is essentially a floating base manipulator operating in an underwater environment, subject to added mass forces, dissipative drag forces, and hydrostatic forces. This allows us to model the USM as an underwater robotic manipulator, with equations of motion given in matrix form by [9], [24]

$$M(q)\dot{\zeta} + C(q,\zeta)\zeta + D(q,\zeta)\zeta + N(R_{Ib}, q) = \tau(q) \tag{19}$$

where $M(q)$ is the system inertia matrix, $C(q,\zeta)$ is the Coriolis-centripetal matrix, $D(q,\zeta)$ is the damping matrix, and $N(R_{Ib}, q)$ is the matrix of gravitational and buoyancy forces. The system inertia matrix is composed of the rigid body inertia matrix $M_{\text{RB}}(q)$ and the added mass inertia matrix, $M_A(q)$, according to $M(q) = M_{\text{RB}}(q) + M_A(q)$. The vector of actuator forces $\tau(q)$ is collocated with ζ and is given by

$$\tau(q) = \begin{bmatrix} \tau_b(q) \\ \tau_q(q) \end{bmatrix} = \begin{bmatrix} T(q) & 0_{6\times n} \\ 0_{n\times m} & I_{n\times n} \end{bmatrix} \begin{bmatrix} u_{thr} \\ u_q \end{bmatrix} \tag{20}$$

where $T(q) \in \mathbb{R}^{6\times m}$ is the TCM, $u_{\text{thr}} \in \mathbb{R}^m$ is the vector of thruster forces, and $u_q \in \mathbb{R}^n$ represents the joint torques.

We can find an expression for the rigid body inertia matrix of the USM as a whole, M_{RB}, by considering the kinetic energy of each link. Equation (17) gives the velocities of the CM of each link with respect to the inertial frame. Thus, we can write the kinetic energy of the links as

$$\begin{aligned} \mathscr{K}_i &= \frac{1}{2}(V_{Ii}^i)^T I_i V_{Ii}^i \\ &= \frac{1}{2}\zeta^T J_{g,i}^T(q) I_i J_{g,i}(q)\zeta \\ &= \frac{1}{2}\zeta^T M_i(q)\zeta \end{aligned} \tag{21}$$

where $I_i \in \mathbb{R}^{6\times 6}$ is the inertia matrix of link i in frame $\mathscr{F}_i$, and superscript T denotes the transpose. The definition of the reference frame $\mathscr{F}_i$ implies that I_i is diagonal. The matrix $M_i(q) = J_{g,i}^T(q) I_i J_{g,i}(q)$ is the inertia matrix of link i expressed with respect to the base of the USM. With all the link inertia matrices expressed in the same frame, we find the total rigid body inertia matrix by summing the contributions of each link as follows:

$$\begin{aligned} M_{\text{RB}}(q) &= \sum_{i=0}^{n} M_i(q) \\ &= \sum_{i=0}^{n} \begin{bmatrix} Ad_{g_{bi}}^{-T} I_i Ad_{g_{bi}}^{-1} & Ad_{g_{bi}}^{-T} I_i Ad_{g_{bi}}^{-1} J_i \\ J_i^T Ad_{g_{bi}}^{-T} I_i Ad_{g_{bi}}^{-1} & J_i^T Ad_{g_{bi}}^{-T} I_i Ad_{g_{bi}}^{-1} J_i \end{bmatrix} \\ &= \begin{bmatrix} M_{11} & M_{12} \\ M_{21} & M_{22} \end{bmatrix}. \end{aligned} \tag{22}$$

The upper-left part $M_{11} \in \mathbb{R}^{6\times 6}$ represents the inertia of the USM as a single rigid body, while the upper right part $M_{12} \in \mathbb{R}^{6\times n}$ is the inertia matrix for the coupling between the joint motion and the USM base. The expression for M_{11} will be used in Section IV-B.

D. Thruster Configuration Matrix

The TCM $T(q)$ in (20) is state dependent, i.e., it is a function of the joint angles. The relative position and orientation of the thrusters with respect to the base of the USM change with the moving joints. In this section, we employ the results from Section III-B to derive an expression for the TCM.

In Section III-B, we derived the geometric link Jacobian, i.e., the mapping between the velocity state vector ζ and the body-fixed velocities of the links. On the other hand, this Jacobian also maps the forces and moments applied on the links to the joint torques and to the base of the manipulator. Using the same approach, we find the geometric Jacobians for the thruster frames J_{g,t_j}, which transfers the forces and moments τ_{t_j} from the thruster frames $\mathscr{F}_{t_j}$ to the base frame $\mathscr{F}_b$, and the joint torques according to

$$\tau(q) = \sum_{j=1}^{m} J_{g,t_j}^T \tau_{t_j} \tag{23}$$

where $\tau_{t_j} = [1 \quad 0_{1\times 5}]^T u_{\text{thr},j}$, and $u_{\text{thr},j}$ is the scalar force applied by thruster j. We are interested in $\tau_b(q)$, the part of $\tau(q)$ acting on the base of the USM. To find this, we use the selection

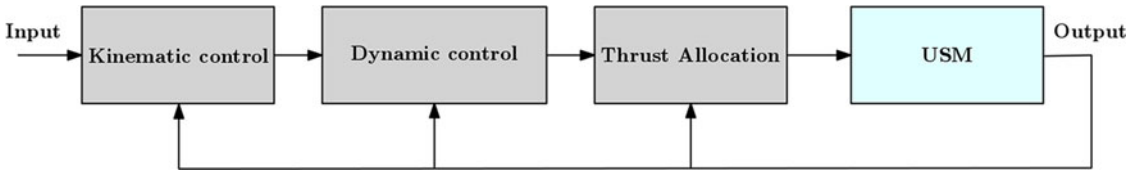

Fig. 5. Motion control framework for the USM.

matrix $H = [I_{6\times 6} \quad 0_{6\times n}]$, which gives

$$\tau_b(q) = H\tau(q) = \sum_{j=1}^{m} H J_{g,t_j}^T(q)\tau_{t_j} = \sum_{j=1}^{m} (Ad_{g_{bt_j}}^{-1})^T \tau_{t_j}. \tag{24}$$

Using (11), we get

$$\tau_b(q) = \sum_{j=1}^{m} B_j(q) u_{thr,j} \tag{25}$$

$$B_j(q) \triangleq \begin{bmatrix} R_{bt_j} & 0 \\ \hat{p}_{bt_j} R_{bt_j} & R_{bt_j} \end{bmatrix} \begin{bmatrix} 1 \\ 0_{5\times 1} \end{bmatrix} \tag{26}$$

which agrees with the equation for transformation of forces and moments from one reference frame to another. By comparing (20) and (25), we see that the TCM $T(q)$ can be expressed as a horizontal concatenation of the column vectors $B_j(q)$.

IV. Motion Control Framework

Realizing operational USMs for underwater inspection and intervention tasks poses a number of complex challenges related to practical issues as well as theoretical aspects such as guidance, control, and computer simulations. In the following sections, we pay particular attention to the topics of kinematic control, dynamic control, and optimal thruster utilization. First, we will describe the USM motion control framework before we go on to discuss in detail each of the main components.

We propose a generic motion control framework for the USM, as shown in Fig. 5. The framework itself resembles a typical guidance, control, and thrust allocation system for marine vehicles. However, the challenges faced by the different subsystems are much more complex for a USM, due to kinematic redundancy, multibody dynamics, dynamic coupling effects, and a state-dependent TCM. The main responsibilities of each subsystem are described as follows.

1) Kinematic control: It generates the reference signals to the joint controllers and the dynamic controller for the overall pose of the USM.
2) Dynamic control: It calculates the joint torques and the generalized forces and moments on the USM, based on the reference signals from the kinematic control module.
3) Thrust allocation: It optimally distributes the generalized forces and moments among the thrusters.
4) USM: It is the physical or simulated model of the USM.

In Sections IV-A, IV-B, and IV-C, each part of the framework will be discussed in details, describing step by step the further development of the concepts initially presented in [7].

A. Kinematic Control

The purpose of the kinematic control module is to coordinate the joint motions and the overall motion of the USM. The primary task for the USM will typically be to control the motion of the end-effector. This can be achieved either by moving the whole USM as a rigid body using the thrusters, by changing the joint angles, or a combination of both. Thus, there are multiple solutions for achieving the desired end-effector pose. Solving this redundancy problem is referred to as redundancy resolution. The redundancy can be utilized to determine the optimal motion of the USM considering one or more optimization criteria, or to fulfill multiple tasks simultaneously. We propose the following list of secondary tasks for USMs, in the prioritized order.

1) Satisfy the mechanical constraints, e.g., maximum joint deflections and maximum angular velocity for the joints.
2) Maintain good manipulability, i.e., avoid singular joint configurations.
3) Maintain controllability, i.e., avoid singular thruster configurations.
4) Avoid collision with other moving objects and stationary obstacles.
5) Minimize the energy consumption.

The reasoning for this choice of priority is that, first of all, it is important not to exceed the physical limitations of the articulated structure, as this may lead to loss of controllability and/or instability. Objective 1) is therefore a prerequisite for achieving the subsequent objectives. Furthermore, exceeding the physical limitations may break the mechanical joints or subject the robot to extensive wear and tear. Second, it is important to avoid singular joint and thruster configurations to maintain good manipulability and controllability, particularly to perform high precision manipulation tasks, station-keeping, and maneuvers in tight spaces. This objective is also a prerequisite for collision avoidance, which is the fourth objective and which is important for the safety of the system and for the environment it works in. Finally, we want to minimize the total energy consumption to extend the intervals between battery recharging.

Inverse kinematic control methods are versatile and widely used tools for redundancy resolution for both fixed-base and floating-base robots. As mentioned in Section I, inverse kinematic control of UVMSs has been studied extensively. Although the USM may seem quite similar to a UVMS, there are some important differences related to kinematic control as follows.

1) The UVMS has a relatively large main body compared to the attached manipulator arm, while the USM is a manipulator arm in itself, without a specific main body. As such, the USM can, in general, utilize all available degrees of freedom, while the UVMS may have to restrict the motion

of the main body to conserve power and to keep the roll and pitch angles close to zero.

2) The use of a singularity free representation is more important for a USM, since the pitch angles of the links may not be restricted, which is typically the case for the main body of the UVMS.
3) The metacentric stability of the UVMS is much larger than for the USM, due to a larger displacement between the center of gravity and the center of buoyancy. This means that the overall roll motion of the USM will be larger, which will have a significant effect on the positioning tasks.
4) For a UVMS, the position and orientation of the thrusters are usually fixed with respect to the main body, while the thruster configuration of the USM is state dependent, i.e., it depends on the joint angles.
5) The dynamic coupling between the motion of the joints and the overall orientation of the USM is quite significant and should be considered also at the kinematic level.

Next, we show how to resolve the kinematic redundancy for single tasks, and how to combine multiple tasks to achieve compound behaviors.

1) Solving Individual Tasks: The tasks are typically defined by task variables $\sigma_i(t)$ to be controlled to a specific value (equality tasks) or to be kept within a defined set (set-based tasks). A comprehensive collection of possible tasks for underwater robotic vehicles is presented in [24]. Determining the motion of the USM required to fulfill the different tasks is conveniently done at the velocity level. Differentiating the expressions for the task variables σ_i with respect to the configuration variables of the system gives the task Jacobians J_i and the relation

$$\dot{\sigma}_i = J_i \zeta. \tag{27}$$

By using a closed-loop inverse kinematics algorithm, the reference velocity components $\zeta_{r,i}$ can be resolved for each task independently by

$$\zeta_{r,i} = J_i^+ \left(\dot{\sigma}_{i,d} - \Lambda_i \tilde{\sigma}_i\right) \tag{28}$$

where the desired task values are represented by $\sigma_{i,d}$, $\tilde{\sigma}_i = \sigma_{i,d} - \sigma_i$ are the task errors, and Λ_i is a diagonal gain matrix. The pseudoinverse of the task Jacobian J_i^+ is given by $J_i^+ = J_i^T (J_i J_i^T)^{-1}$. To prioritize or disregard certain control inputs, the weighted pseudoinverse $J_i^\dagger = W_i^{-1} J_i^T (J_i W_i^{-1} J_i^T)^{-1}$ can be used instead. The weighted pseudoinverse solution corresponds to solving the following least-squares optimization problem:

$$\min_{\zeta_{r,i}} \left\{ \zeta_{r,i}^T W_i \zeta_{r,i} \right\} \tag{29}$$

$$\text{subject to:} \quad J_i \zeta_{r,i} = \dot{\sigma}_{i,d}.$$

By setting a diagonal element of the weighting matrix W_i to a very high value, the corresponding control input is effectively disregarded. This can be desirable for instance if a joint mechanism is out of order or if the given task should be satisfied without using the pitch and roll axes of the USM. Weighting can also be used to avoid joint limits by specifying the elements of W_i as functions that approach infinity as the joint angles get close to their respective limits.

For certain configurations of the USM, the task Jacobians can become ill-conditioned, which means that the matrices $J_i W_i^{-1} J_i^T$ become close to singular. Such singular configurations are termed kinematic singularities, and are associated with loss of control over the task variable. Trying to invert a near-singular matrix leads to excessively high joint velocity commands and may cause instability. To avoid this, we relax the strict requirement of satisfying the task by solving the modified optimization problem

$$\min_{\zeta_{r,i}, s_i} \left\{ \zeta_{r,i}^T W_i \zeta_{r,i} + s_i^T Q_i s_i \right\} \tag{30}$$

$$\text{subject to:} \quad J_i \zeta_{r,i} = \dot{\sigma}_{i,d} + s_i$$

where the slack variable s_i is introduced in the cost function with an appropriate weighting $Q \gg 0$, such that s_i is only allowed to increase when the optimum solution would otherwise yield unfeasible reference velocities. Increasing the slack variable s_i is equivalent to relaxing the hard constraint of satisfying the task and thus, a deviation from the specified task value will occur. The explicit minimum norm solution is given by

$$\zeta_{r,i} = W_i^{-1} J_i^T \left(J_i W_i^{-1} J_i^T + Q_i^{-1} \right)^{-1} \dot{\sigma}_{i,d}. \tag{31}$$

If we set $W_i = I$ and $Q_i = (1/\lambda^2) I$, then (31) is reduced to the standard damped least-squares solution. Set-based tasks can also be used to avoid kinematic singularities. In [12], this approach was employed for kinematic singularity avoidance for the primary end-effector task.

2) Combining Multiple Tasks: Here, we show how to apply the SRMTP method for simultaneous kinematic redundancy resolution of multiple tasks. The SRMTP approach is a task-based method, originating from the well-known task priority method [13], [45]. The task priority method handles multiple tasks with strict prioritization, which means that each task will be fulfilled in a prioritized order. The SRMTP approach is a modification of the original task priority method to avoid the occurrence of algorithmic singularities caused by conflicting tasks, hence the name singularity-robust task priority. Using the SRMTP approach, lower priority tasks will only create internal self-motions that do not interfere with the higher priority tasks. The generic expression for the SRMTP method with k tasks assigned to different priority levels is

$$\begin{aligned} \zeta_r = {} & J_1^+ \left(\dot{\sigma}_{1,d} + \Lambda_1 \tilde{\sigma}_1\right) + N_1 J_2^+ \left(\dot{\sigma}_{2,d} + \Lambda_2 \tilde{\sigma}_2\right) \\ & + \cdots + N_{12..(k-1)} J_k^+ \left(\dot{\sigma}_{k,d} + \Lambda_k \tilde{\sigma}_k\right) \end{aligned} \tag{32}$$

where $\zeta_r = [(V_{Ib,r}^b)^T, q_r^T]^T$ is the velocity reference vector. The null spaces of the task Jacobians are given by $N_i = (I - J_i^\dagger J_i)$, while $N_{12..(k-1)}$ represents the combined null space of tasks 1 through $k-1$. The null space matrices ensure that conflicting velocity components generated by the lower priority tasks are filtered out. Each defined task for the USM can be solved individually, by the methods explained above, and then combined in a prioritized order using (32). The outputs from the SRMTP algorithm are the velocity reference vector for the USM base $V_{Ib,r}^b$ and the joint velocity reference vector, q_r. In Section IV-B,

we discuss the dynamic control law, whose responsibility is to track the reference motion for the base of the USM.

B. Dynamic Control

The dynamic control module takes care of calculating the required forces and moments on the base of the USM, based on the input from the kinematic control module. A simple proportional control law was used in [6] for planar straight line path following, and in [7] for station-keeping combined with the inverse kinematic control in 2-D. In this paper, we propose to use a state-feedback linearization controller to track the body-fixed reference velocity for the USM base $V^b_{Ib,r}$ generated by the kinematic control module. The control law is given by

$$\tau_c = M_{11}(q)a^b + n(R_{Ib}, q, \zeta) \tag{33}$$

where τ_c is the vector of commanded generalized forces and moments, $M_{11}(q)$ is found by (22), and a^b is the commanded body-fixed acceleration vector given by

$$a^b = \dot{V}^b_{Ib,r} - K_P\tilde{V}^b_{Ib} - K_I\int_0^t \tilde{V}^b_{Ib}(\tau)d\tau. \tag{34}$$

The velocity tracking error is $\tilde{V}^b_{Ib} = V^b_{Ib} - V^b_{Ib,r}$, K_P and K_I are diagonal positive definite gain matrices, and the nonlinear feedback linearization matrix $n(R_{Ib}, q, \zeta)$ is given by

$$n(R_{Ib}, q, \zeta) = C_{11}(q, \zeta)\zeta + D_{11}(q, \zeta)\zeta + N_{11}(R_{Ib}, q) \tag{35}$$

where $C_{11}(q, \zeta)$, $D_{11}(q, \zeta)$, and $N_{11}(R_{Ib}, q)$ are specified as the upper-left submatrices of the corresponding matrices in (19). Inserting (33) into (19) yields a linear closed-loop system, and the gain matrices can be calculated using conventional pole placement techniques [23]. The proposed control law is applied in Section VI to perform combined simulations with both kinematic and dynamic control. In this paper, we choose not to include torque control of the joints, as the joint motors are typically controlled by a built-in low-level proportional controller.

A future topic of interest is to investigate more sophisticated control approaches that take into account uncertainties in the hydrodynamic parameters, ocean current disturbances, and the dynamic coupling between the motion of the joints and the overall motion of the USM. Some control approaches that may be applicable to USMs are the mixed frame adaptive control law in [46] and [47], the virtual decomposition approach in [48] and [49], and the energy efficient method suggested in [50].

C. Thrust Allocation

Thrust allocation is the process of distributing the commanded generalized forces and moments between the thrusters. For a typical UVMS, each thruster has a fixed position and orientation relative to the body-fixed reference frame. The thrusters are usually mounted in pairs and aligned with the axes of rotation, such that they affect only the axes that needs to be controlled. However, this is not the case for the USM. When the shape of the USM is changed, the position and orientation of each thruster with respect to the base of the USM are also changed. Consequently, the TCM may become singular, and the thrust allocation algorithm must therefore take this into account to maintain control of the USM. Near-singular thruster configurations are associated with excessively high thruster commands. In such configurations, it is necessary to allow the thrusters to deviate from the thrust command τ_c. A simple but effective way of doing this is to solve the minimization problem

$$\min_{u_{\text{thr}}} \left(\lambda^2||u_{\text{thr}}||^2 + ||T(q)u_{\text{thr}} - \tau_c||^2\right) \tag{36}$$

where λ is a suitably chosen damping factor, which may be constant or configuration dependent. This is an unconstrained quadratic optimization problem, where the goal is to minimize the norm of the thruster efforts and the norm of the deviation from the thrust command. The damping factor λ should preferably be chosen as a small value, such that the relative importance of satisfying the specified thrust command τ_c becomes high. The explicit solution to (36) is given by

$$u_{\text{thr}} = T^\dagger(q)\tau_c \tag{37}$$

where $T^\dagger(q) = T(q)^T\left(T(q)T(q)^T + \lambda^2 I\right)^{-1}$ is called the damped pseudoinverse of $T(q)$. This solution is applied for the simulations in Section VI.

If the USM has more thrusters than required to satisfy the given control task, it is referred to as an overactuated system. In this case, the solution to the thrust allocation problem is not unique, i.e., there are infinite solutions for distributing the thruster forces and yet obtain the same generalized forces and moments. Typically, an optimization-based algorithm is then applied to solve the allocation problem in an optimal manner, based on various criteria and constraints. For the USM, we propose the following alternatives as optimization criteria:

1) minimize a measure of the combined thruster efforts;
2) minimize the single largest thruster force;
3) minimize the thruster force fluctuations.

The purpose of the criteria to minimize the combined thruster efforts is to reduce the overall power consumption, while minimizing the single largest thruster force aims at utilizing the thrusters equally. Keeping the thruster force fluctuations as low as possible is important to avoid unnecessary wear and tear. Typical constraints are related to the physical limitations of the thrusters, including maximum forward and reverse thrust, and maximum RPM speed of change. It is possible to also consider the joint angles as optimization variables, with the goal of obtaining a more efficient thruster configuration. In that case, the optimization problem becomes nonconvex and much more difficult to solve in real time.

In this paper, we focus mainly on illustrating the applicability of the proposed motion control framework. We have, therefore, chosen a simplified unconstrained thrust allocation method for the USM, with the combined thruster efforts as the optimization criteria. The physical limitations of the thrusters are taken into account by tuning the gains of the dynamic control law. This ensures that the thrust command τ_c is kept below the attainable limits.

V. Modes of Operation

The USM is effectively a floating base manipulator. As such, the USM can transport itself to an area of interest, perform

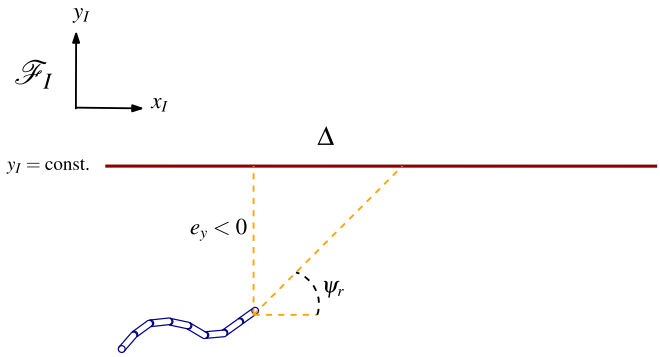

Fig. 6. LOS guidance law.

an inspection or intervention task, and then return to its home position. Sverdrup-Thygeson *et al.* [7] proposed to divide this sequence of operations into two distinct modes of operation, namely, transport mode and work mode. In this section, we complement the previous discussion of the transport mode and the work mode, and we propose kinematic control strategies tailored for each mode.

A. Transport Mode

The primary objective of the transport mode is to move the USM to a target position, while traveling along a specified path. In this paper, we consider a simplified path following problem where the goal is to make the USM converge to a straight line path in a 2-D horizontal plane. We define the heading of the USM ψ to be the heading of the front link in the inertial frame, and we use a simple but effective joint control strategy first proposed in [6] and more recently used in the experiments in [51]. The joint reference angles are set according to

$$q_{r,i} = k_\psi(\psi - \psi_r) \tag{38}$$

where $k_\psi > 0$ is a control gain. In this paper, we consider a straight line path parallel to the inertial frame *X*-axis. The reference heading ψ_r can then be determined by a line-of-sight (LOS) guidance algorithm given by

$$\psi_r = -\arctan\left(\frac{e_y}{\Delta}\right) \tag{39}$$

where $\Delta > 0$ is the look-ahead distance, and e_y is the cross-track error, i.e., the minimum distance from the front of the USM to the straight line. The relationship in (39) is visualized in Fig. 6. This LOS guidance law is commonly used for path following control of marine surface vessels [52], [53], and it has also been used for path following for USRs without thrusters in [54]. As long as the vehicle maintains a nonzero forward velocity and in the absence of ocean current disturbances, the LOS guidance law ensures convergence to the straight line path. Since the USM can use both the joints and the thrusters to turn toward the path, we conjecture that we can choose a smaller look-ahead distance than the typical value of two times the vehicle length, and thus obtain faster convergence to the path.

To calculate the commanded forces and moments, we apply the dynamic control law in (33), with a slight modification of the desired body-fixed acceleration vector in (34). The commanded surge and yaw accelerations are calculated according to

$$a_1^b = -k_{1,P}(u - u_c) - k_{1,I}\int(u - u_c) \tag{40}$$

$$a_6^b = -k_{6,D}(\dot{\psi} - \dot{\psi}_r) - k_{6,P}(\psi - \psi_r) \tag{41}$$

where $k_{1,P}$, $k_{1,I}$, $k_{6,D}$, and $k_{6,P}$ are scalar control gains, u is the surge component of the end-effector velocity V_{Ie}^e, and u_c is the commanded surge velocity. The remaining acceleration components are set to zero. Simulation results for transport mode using this control strategy is presented in Section VI-B.

B. Work Mode

The work mode is primarily intended for inspection and intervention tasks that require station-keeping and low-speed maneuvering capabilities. The main objective in work mode will typically be to control the pose and the velocity of the USM end-effector, while trying to satisfy the secondary objectives listed in Section IV-A. Additional specific criteria such as minimum distance to the seafloor and desired view angles of attached cameras can be included. The SRMTP method discussed in Section IV-A is well suited for handling multiple objectives.

Deriving the end-effector Jacobian by differentiation of the forward kinematics becomes cumbersome for a serial robotic mechanism with many links like the USM. Therefore, we apply the method described in Section III-B to find the end-effector Jacobian $J_{g,e}(q)$ directly. Another advantage of using (18) to find $J_{g,e}(q)$ is that the expression is free from representation singularities, which is not the case when Euler angles are used as task variables to represent the pose of the end-effector. Using the SRMTP method, we resolve the reference velocities for the joints and the base of the USM by

$$\zeta_r = J_{g,e}^\dagger(q)\left(V_{Ie,d}^e + k_e\tilde{e}_e\right) + \left(I - J_{g,e}^\dagger(q)J_{g,e}(q)\right)J_b^+ k_b\tilde{p}_b \tag{42}$$

where $k_e > 0$ and $k_b > 0$ are control gains, $V_{Ie,d}^e$ is the desired end-effector velocity, and $\tilde{e}_e = \left[\tilde{p}_e^T, \tilde{\epsilon}_e^T\right]^T$ is the end-effector error vector. The position deviations of the end-effector and the USM base are given by $\tilde{p}_e$ and $\tilde{p}_b$, respectively, and $\tilde{\epsilon}_e$ is the vector part of the quaternion representation of the end-effector orientation deviation. The base frame Jacobian J_b is given by $J_b = [R_{Ib} \quad 0_{3\times(n+3)}]$. Note that we use the weighted pseudoinverse of $J_{g,e}(q)$ to prioritize the use of the joints to fulfill the primary end-effector task. The secondary task aims at keeping the USM base stationary at a *home* position, while carrying out the instructed inspection or intervention task. Additional equality or set-based tasks can easily be included to satisfy, e.g., joint limit constraints and objectives such as kinematic singularity avoidance [12], obstacle avoidance, and camera view angles. Simulation results using (42) to determine the reference velocities are presented in Section VI-C.

VI. Simulations

In this section, we present simulations in 3-D combining the elements of the proposed motion control framework, including motion coordination based on inverse kinematics, dynamic

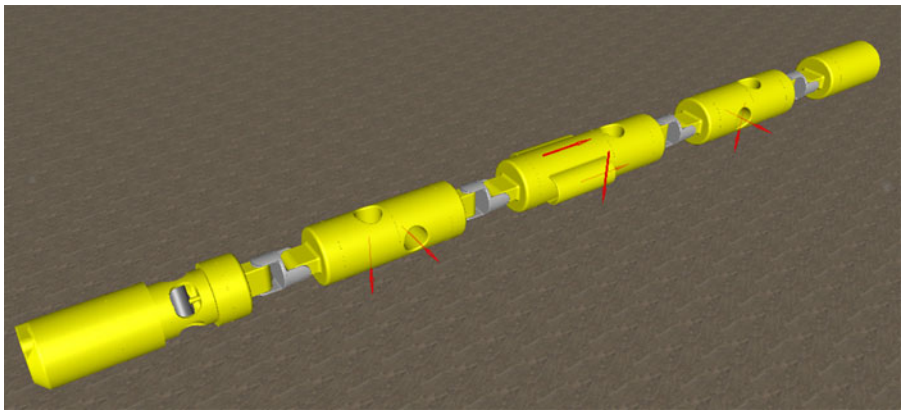

Fig. 7. Vortex simulation model.

control, and thrust allocation. This extends the 2-D simulations performed in [7] and the pure kinematic simulations performed in [8].

In [6] and [7], simulations were carried out in 2-D using an analytical model of the USM implemented in MATLAB. To extend this to 3-D, we established, in [8], a simulation environment using MATLAB/Simulink and the multibody dynamic simulation tool Vortex by CM Labs, Montreal, QC, Canada [33]. This setup enables real-time simulation and testing under realistic and adjustable hydrodynamic and hydrostatic conditions, and provides a powerful and flexible way to experiment with different control algorithms, control parameters, and physical designs, e.g., number of links and various thruster configurations. The control algorithms are implemented in MATLAB and communicate with Vortex through a generic Simulink interface. Next, we explain the development of the new Vortex simulation model of a fully actuated USM, which replaces the preliminary model presented in [8].

A. Vortex Simulation Model

We have developed a simulation model in Vortex of a fully actuated USM, to demonstrate the applicability of the motion control framework proposed in Section IV. In this section, we describe the development process and each element of the model. As visualized in Fig. 7, the USM model consists of five links, where each link is connected to its neighbor by two 1-DOF joints. In addition, the model is equipped with a total of seven thrusters. The overall process of developing the Vortex model can be described as follows.

1) Model each component in the CAD tool Solidworks.
2) Import models in Vortex as graphical geometries.
3) Merge all geometries that form rigid connections together.
4) Reduce the number of vertices and meshes using a built-in function in Vortex.
5) Create parts in Vortex corresponding to each geometry, and specify properties such as mass, CM, moment of inertia, and added mass.
6) Create 1-DOF hinges, and specify which parts to attach and the axes of rotation.
7) Create convex fluid interaction geometries enclosing each part, and specify buoyancy properties and drag coefficients.
8) Create attachment points for each thruster.
9) Create thruster objects, connect them to the attachment points, and specify the direction of the applied thruster force.
10) Create a simulation scene representing the underwater environment and place the USM mechanism in the scene.

For simplicity, the Vortex model of the USM is designed to be neutrally buoyant, with both CM and center of buoyancy set to the volumetric center of the parts. The mass is assumed to be homogeneously distributed, such that the moment of inertia can be calculated according to standard expressions for cylindrical objects. Moreover, the added mass matrix for each part is assumed to be diagonal and specified according to [55]

$$M_{A_{11}} = 10\% \text{ of mass} \qquad M_{A_{44}} = 0$$

$$M_{A_{22}} = \pi\rho r_i^2 l_i \qquad M_{A_{55}} = \frac{1}{12}\pi\rho r_i^2 l_i^3$$

$$M_{A_{33}} = \pi\rho r_i^2 l_i \qquad M_{A_{66}} = \frac{1}{12}\pi\rho r_i^2 l_i^3$$

where $\rho = 1026\,\text{kg/m}^3$ is the seawater density, and r_i and l_i represent the radius and length of each part, respectively.

In Vortex, the drag coefficients can be specified separately for the *X*, *Y*, and *Z* axes of each part to adapt to different shapes and surface roughness, as well as to account for parts that are partially concealed behind other parts. In the absence of experimental data, we have set the drag coefficients to typical values for blunt cylindrical objects with a large length to diameter ratio [55], [56]. Due to slow motion of the USM, we assume that the Reynolds number is $Re < 2e5$, and that the USM operates under laminar flow conditions. Furthermore, the *X*-axis coefficients for the joints and the middle links are adjusted to account for partial concealment, which reduces the pressure drag component significantly. The remaining drag is due to skin friction. Some common properties of the model parts are listed in Table II.

The joint limits are $\pm 90^\circ$, and the maximum thruster force is set to 40 N per thruster. The thrusters in Vortex accept RPM commands as input, and map this to instantaneous point forces

TABLE II
USM MODEL PROPERTIES

Property	Link 0	Joint 1	Link 1	Joint 2	Link 2	Joint 3	Link 3	Joint 4	Link 4
Dry mass [kg]	14.3	6.0	12.7	6.0	9.8	6.0	12.7	6.0	7.8
Wet mass [kg]	0.0	0.0	0.0	0.0	0.0	0.0	0.0	0.0	0.0
Length [m]	0.62	0.104	0.584	0.104	0.726	0.104	0.584	0.104	0.37
Radius [m]	0.085	0.085	0.085	0.085	0.085	0.085	0.085	0.085	0.085
Drag coeff. (x, y, z)	$\begin{pmatrix}0.8\\1.0\\1.0\end{pmatrix}$	$\begin{pmatrix}0.1\\1.0\\1.0\end{pmatrix}$	$\begin{pmatrix}0.1\\1.0\\1.0\end{pmatrix}$	$\begin{pmatrix}0.1\\1.0\\1.0\end{pmatrix}$	$\begin{pmatrix}0.1\\1.0\\1.0\end{pmatrix}$	$\begin{pmatrix}0.1\\1.0\\1.0\end{pmatrix}$	$\begin{pmatrix}0.1\\1.0\\1.0\end{pmatrix}$	$\begin{pmatrix}0.1\\1.0\\1.0\end{pmatrix}$	$\begin{pmatrix}0.8\\1.0\\1.0\end{pmatrix}$

through a static piecewise linear mapping. This means that the response time between the thrust command and the actual thrust output is not modeled. This limitation can be circumvented by filtering the desired motion trajectories to ensure that the rate of change of the commanded forces and moments do not exceed typical thruster performance limitations. The position of the thrusters are chosen to ensure that the USM remains fully actuated in nearly all configurations. An exception is when the USM assumes a straight body shape. In this configuration, the TCM drops rank and the ability to control the roll motion of the USM is lost. Nonetheless, this is not considered as a problem, since the camera in the front link of the USM is suspended such that the camera roll angle always remains zero. Also, as explained in Section IV-C, we apply a damped thrust allocation method, such that excessive thruster forces are avoided when the TCM is ill conditioned. Sections VI-B and VI-C present the simulation results from the combined kinematic and dynamic simulations of both transport mode and work mode.

B. Transport Mode Simulation

In this section, we present simulation results for transport mode using the control strategy described in Section V-A. We compare two slightly different methods based on the same set of equations. In method 1, the thrusters are used to control the end-effector surge velocity, while in method 2 the surge velocity of the USM base is being controlled. In other words, method 1 resembles the case of trying to drag the USM through the water by its head, while method 2 corresponds to pushing at the back end of the USM. The simulations are set up to make the USM follow a sequence of straight line segments parallel to the inertial frame *X*-axis, as shown by the dashed blue lines in Fig. 8(a) and (b). At time $t = 95$, the USM is instructed to make a 180° turn. Table III lists the control parameter values, which are obtained through trial and error.

By comparing Fig. 8(a) and (b), we see that method 2 provides faster convergence to the desired path with less overshoot than method 1. Fig. 8(b) also shows that the back end of the USM follows the trajectory of the front end more closely, while in Fig. 8(a) the back end has a more pendulum-like motion. The faster convergence of method 2 requires higher sideways velocity of the USM end-effector, as shown by the solid red lines in Fig. 8(c) and (d). The motion of the joints, visualized in Fig. 8(e) and (f), exhibits no significant differences. Regarding the use of the thrusters, we notice from Fig. 8(g) and (h) that the thruster forces are far below the upper limit of 40 N, except during the 180° turn, when the sideways thrusters are used to assist the turning of the USM. Fig. 8(h) shows that method 2 uses slightly more thruster effort. This is related to the faster convergence and a higher value of the control gain $k_{6,P}$ for the yaw motion. The low thruster efforts during transport mode indicate that the USM is capable of performing long distance transits and long surveillance operations, even with limited battery capacity. The simulations presented here indicate that method 2 is the more appropriate of these two methods for straight line path following of USMs. However, more simulations and experimental testing are needed to confirm this.

TABLE III
TRANSPORT MODE CONTROL PARAMETERS

	u_c	Δ	k_ψ	$k_{1,P}$	$k_{1,I}$	$k_{6,D}$	$k_{6,P}$
method 1	0.5	3	0.45	0.5	0.0625	0.13	0.12
method 2	0.5	2	0.45	0.5	0.0625	0.01	0.2

C. Work Mode Simulation

In this section, the desired motion of the end-effector is specified as a time-invariant setpoint regulation task. We presume that the position and orientation setpoints are given by a human operator or by a high-level task controller. The end-effector setpoints are specified in 6 DOF, visualized by the dashed lines in Fig. 9(a) and (b). The joint velocity references $\dot{q}_r$ and the reference base frame velocity $V^b_{Ib,r}$ are calculated by the SRMTP kinematic control law in (42), with parameter values $k_e = \text{diag}([0.2, 0.2, 0.2, 0.4, 0.4, 0.4])$ and $k_b = \text{diag}([0.15, 0.15, 0.15])$. We utilize all the DOFs of the USM, except the roll motion of the USM base, to make the end-effector converge to the setpoints. The use of the different DOFs is weighted using $W = \text{diag}([0.3, 0.3, 0.3, 0.0, 0.3, 0.3, 0.7, 0.7, 1, 1, 1, 1, 1, 1])$ in the computation of the weighted pseudoinverse of the end-effector Jacobian, $J^\dagger_{g,e}(q)$. This weighting matrix means that we prioritize the use of the joints to solve the end-effector setpoint task. The roll motion is excluded in the SRMTP method by setting the fourth diagonal element of W to zero. The joint velocity references are integrated to joint angle references, which are then set directly in the Vortex simulation tool.

Next, the forces and moments to be applied to the USM base are computed by (33) without the nonlinear term, and using $K_P = \text{diag}([1, 1, 1, 0, 1, 1])$ and no integral effect. We justify this simplification by the fact that the simulation model

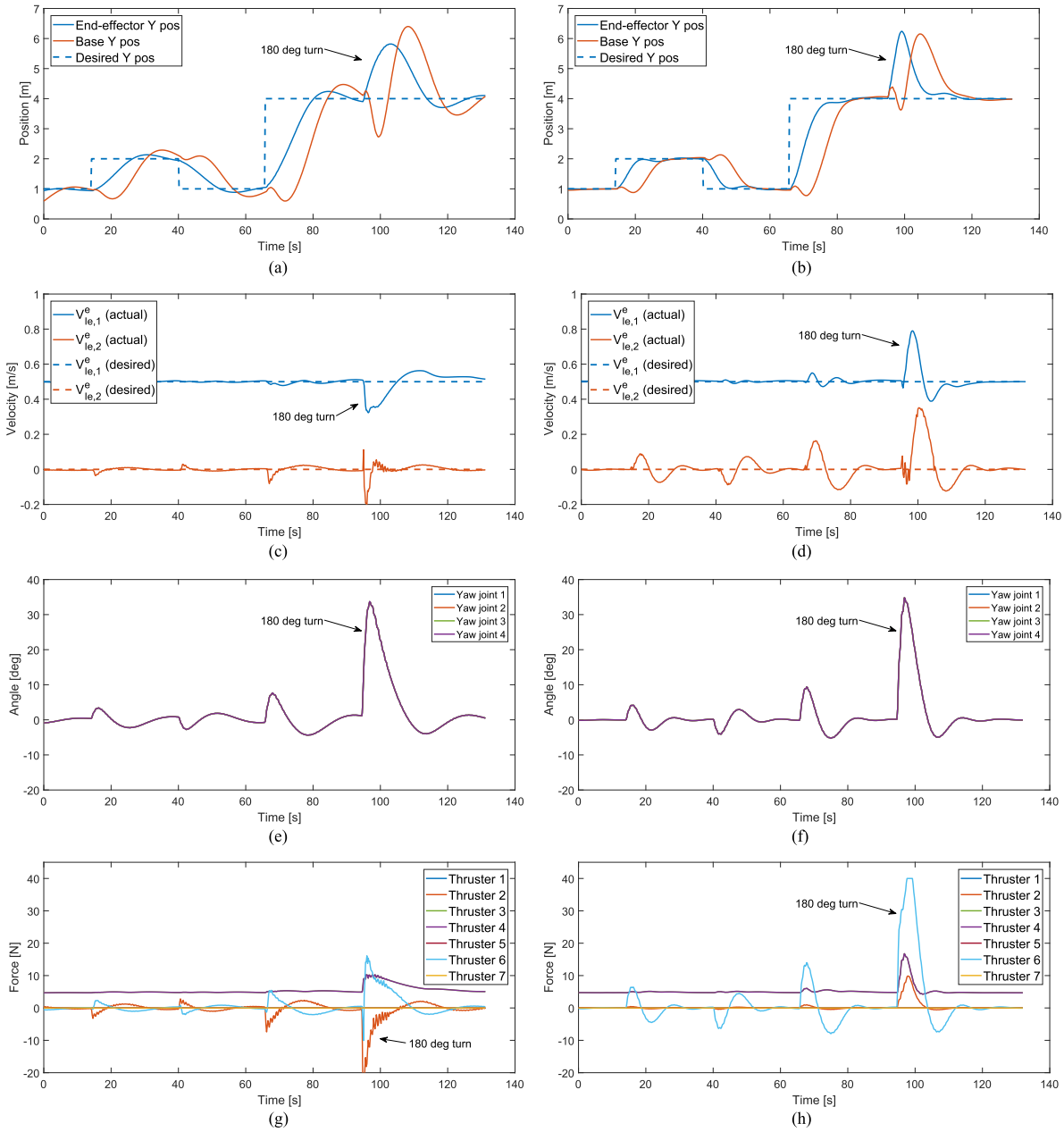

Fig. 8. Simulation results for transport mode. (a) method 1: Y position. (b) method 2: Y position (c) method 1: End-effector velocity. (d) method 2: End-effector velocity. (e) method 1: Joint angles. (f) method 2: Joint angles. (g) method 1: Thruster forces. (h) method 2: Thruster forces.

is neutrally buoyant, and that the Coriolis-centripetal forces and the drag forces are dominated by the inertial forces and the added mass forces due to slow velocities when operating in work mode. Note that the fourth diagonal element of K_P is set to zero, which means we do not attempt to control the roll motion of the USM base. Finally, the distribution of the thruster forces is found by (37) with damping factor $\lambda = 0.1$. The control parameters are found through trial and error.

Fig. 9(a) and (b) shows that the end-effector pose converges to the setpoints, except the roll angle of the end-effector, which fluctuates around its desired value. Despite this deviation from the roll setpoint, the camera in the front link of the USM will deliver a level video feed, since it is mounted on a self-leveling mechanism. Fig. 9(e) indicates that the joints are used extensively to fulfill the tasks. The linear and angular velocities of the base are shown in Fig. 9(c) and (d), and we observe that the base follows the reference velocities quite well, despite the use of a simplified dynamic controller. There is some deviation in the roll motion of the base, which is caused by our choice to neglect this DOF in the control law. The distribution of the thruster forces is shown in Fig. 9(f). We expect to see a reduction in the overall performance of the USM, when including thruster dynamics in the simulation model. However, it may be possible to compensate for this using more sophisticated dynamic control laws.

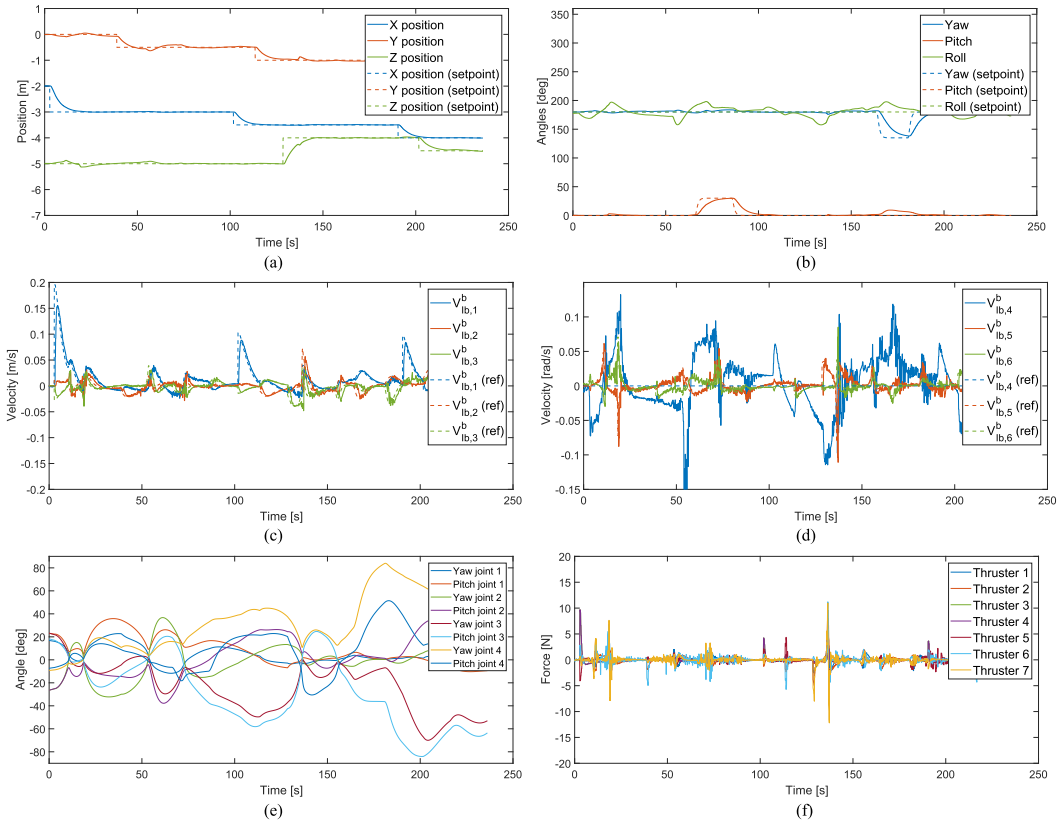

Fig. 9. Simulation results for work mode. (a) End-effector position. (b) End-effector orientation. (c) Linear velocity of the base. (d) Angular velocity of the base. (e) Joint angles. (f) Thruster forces.

This simulation indicates that the proposed motion control framework, separating the kinematic redundancy resolution from the dynamic control, is suitable for controlling a USM operating in work mode.

VII. Conclusion

In this paper, we have discussed the advantages of the innovative USM, and thoroughly explained how this bioinspired AUV can complement existing solutions and contribute to carry out lighter subsea IMR operations. We have summarized and extended the previous research on USMs to provide a clear and consistent overview and to act as a foundation for future work. The derivation of the kinematic and the dynamic model of the USM has been explained in detail, together with the derivation of the state-dependent TCM. Moreover, a generic framework for motion control of the USM has been proposed, and each component of the framework has been discussed in-depth. In particular, two modes of operation, with distinct control strategies, have been proposed, and combined kinematic and dynamic simulations have been performed for both modes. The simulation results provide strong support for the applicability of the proposed motion control framework for guidance and control of USMs.

To further enhance the performance of the USM, and to demonstrate the superior flexibility and accessibility, more sophisticated control strategies will be investigated. Adding thruster dynamics to the simulation model and comparing the energy consumption to that of an ROV, are also considered as future topics of interest.

References

[1] B. Gilmour, G. Niccum, and T. O'Donnell, "Field resident AUV systems - Chevron's long-term goal for AUV development," in *Proc. IEEE/OES Auton. Underwater Veh.*, Southampton, U.K., Sep. 24–27, 2012, pp. 1–5.

[2] Autonomous Inspection Vehicle (AIV). Subsea 7, 2017. [Online]. Available: http://tinyurl.com/jxtc5aw

[3] Seaeye Sabertooth. SAAB, 2017. [Online]. Available: http://tinyurl.com/zhr9rva

[4] Marlin AUV. Lockheed Martin, 2017. [Online]. Available: http://tinyurl.com/jmnhps5

[5] P. J. Sanz, R. Marín, J. Sales, G. Oliver, and P. Ridao, *Recent Advances in Underwater Robotics for Intervention Missions. Soller Harbor Experiments.* Mallorca, Spain: Low Cost Books, 2012.

[6] J. Sverdrup-Thygeson, E. Kelasidi, K. Y. Pettersen, and J. T. Gravdahl, "Modeling of underwater swimming manipulators," *IFAC-PapersOnLine*, vol. 49, no. 23, pp. 81–88, Sep. 2016.

[7] J. Sverdrup-Thygeson, E. Kelasidi, K. Y. Pettersen, and J. T. Gravdahl, "A control framework for biologically inspired underwater swimming manipulators equipped with thrusters," *IFAC-PapersOnLine*, vol. 49, no. 23, pp. 89–96, Sep. 2016.

[8] J. Sverdrup-Thygeson, E. Kelasidi, K. Y. Pettersen, and J. T. Gravdahl, "The underwater swimming manipulator – A bio-inspired AUV," in *Proc. IEEE/OES Auton. Underwater Veh.*, Tokyo, Japan, Nov. 6–9, 2016, pp. 387–395.

[9] P. J. From, J. T. Gravdahl, and K. Y. Pettersen, *Vehicle-Manipulator Systems: Modeling for Simulation, Analysis, and Control* (ser. Advances in Industrial Control). New York, NY, USA: Springer-Verlag, 2014.

[10] Y. Yamamoto and X. Yun, "Coordinating locomotion and manipulation of a mobile manipulator," in *Proc. 31st IEEE Conf. Decision Control*, Tucson, AZ, USA, Dec. 16–18, 1992, pp. 2643–2648.

[11] S. Soylu, B. J. Buckham, and R. P. Podhorodeski, "Redundancy resolution for underwater mobile manipulators," *Ocean Eng.*, vol. 37, no. 2/3, pp. 325–343, 2010.

[12] J. Sverdrup-Thygeson, S. Moe, K. Y. Pettersen, and J. T. Gravdahl, "Kinematic singularity avoidance for robot manipulators using set-based manipulability tasks," in *Proc. 1st IEEE Conf. Control Technol. Appl.*, Mauna Lani, HI, USA, Aug. 27–30 2017, pp. 142–149.

[13] A. Maciejewski and C. Klein, "Obstacle avoidance for kinematically redundant manipulators in dynamically varying environments," *Int. J. Robot. Res.*, vol. 4, no. 3, pp. 109–117, 1985.
[14] N. Sarkar and T. K. Podder, "Motion coordination of underwater vehicle-manipulator systems subject to drag optimization," in *Proc. IEEE Int. Conf. Robot. Autom.*, Detroit, MI, USA, May 10–15, 1999, pp. 387–392.
[15] G. Antonelli and S. Chiaverini, "Task-priority redundancy resolution for underwater vehicle-manipulator systems," in *Proc. IEEE Int. Conf. Robot. Autom.*, Leuven, Belgium, May 16–20, 1998, pp. 768–773.
[16] G. Antonelli and S. Chiaverini, "Singularity-free regulation of underwater vehicle-manipulator systems," in *Proc. Amer. Control Conf.*, Philadelphia, PA, USA, Jun. 24–26, 1998, pp. 399–403.
[17] G. Antonelli and S. Chiaverini, "Fuzzy redundancy resolution and motion coordination for underwater vehicle-manipulator systems," *IEEE Trans. Fuzzy Syst.*, vol. 11, no. 1, pp. 109–120, Feb. 2003.
[18] E. Simetti, G. Casalino, S. Torelli, A. Sperindè, and A. Turetta, "Floating underwater manipulation: Developed control methodology and experimental validation within the TRIDENT project," *J. Field Robot.*, vol. 31, no. 3, pp. 364–385, 2014.
[19] E. Simetti and G. Casalino, "A novel practical technique to integrate inequality control objectives and task transitions in priority based control," *J. Intell. Robot. Syst.*, vol. 84, no. 1, pp. 877–902, 2016.
[20] S. Chiaverini, "Singularity-robust task-priority redundancy resolution for real-time kinematic control of robot manipulators," *IEEE Trans. Robot. Autom.*, vol. 13, no. 3, pp. 398–410, Jun. 1997.
[21] N. Mansard and F. Chaumette, "Task sequencing for high-level sensor-based control," *IEEE Trans. Robot.*, vol. 23, no. 1, pp. 60–72, Feb. 2007.
[22] G. Antonelli, "Stability analysis for prioritized closed-loop inverse kinematic algorithms for redundant robotic systems," *IEEE Transa. Robot.*, vol. 25, no. 5, pp. 985–994, Oct. 2009.
[23] T. I. Fossen, *Handbook of Marine Craft Hydrodynamics and Motion Control*. Hoboken, NJ, USA: Wiley, 2011.
[24] G. Antonelli, *Underwater Robots*, 3rd ed. New York, NY, USA: Springer-Verlag, 2014.
[25] S. Berge and T. Fossen, "Robust control allocation of overactuated ships: Experiments with a model ship," in *Proc. IFAC Conf. Manoeuv. Control Marine Craft*, Brijuni, Croatia, 1997, pp. 166–171.
[26] T. Johansen, T. Fuglseth, P. Tøndel, and T. Fossen, "Optimal constrained control allocation in marine surface vessels with rudders," *Control Eng. Practice*, vol. 16, no. 4, pp. 457–464, 2008.
[27] I. Lindfors, "Thrust allocation method for the dynamic positioning system," in *Proc. 10th Ship Control Symp.*, Ottawa, ON, Canada, 1993, pp. 93–106.
[28] O. J. Sørdalen, "Optimal thrust allocation for marine vessels," *Control Eng. Practice*, vol. 5, no. 9, pp. 1223–1231, 1997.
[29] W. Webster and J. Sousa, "Optimum allocation for multiple thrusters," in *Proc. 9th Int. Offshore Polar Eng. Conf.*, Brest, France, 1999, pp. 83–89.
[30] T. I. Fossen, T. A. Johansen, and T. Perez, 'A survey of control allocation methods for underwater vehicles," in *Underwater Vehicles*. A. V. Inzartsev, Ed. Rijeka, Croatia: InTech, 2008, ch. 7, pp. 109–128.
[31] G. Indiveri and G. Parlangeli, "On thruster allocation, fault detection and accommodation issues for underwater robotic vehicles," in *Proc. Int. Symp. Commun. Control Signal Process.*, Marrakech, Morocco, 2006, pp. 1–4.
[32] T. Johansen and T. Fossen, "Control allocation - A survey," *Automatica*, vol. 49, no. 5, pp. 1087–1103, 2013.
[33] Vortex simulation software. CM Labs Simulations, Inc., 2017. [Online]. Available: https://www.cm-labs.com
[34] J. Evans, K. Keller, J. Smith, P. Marty, and O. Rigaud, "Docking techniques and evaluation trials of the SWIMMER AUV: An autonomous deployment AUV for work-class ROVs," in *Proc. MTS/IEEE OCEANS*, 2001, pp. 520–528.
[35] Y. Chardard and T. Copros, "SWIMMER: Final sea demonstration of this innovative hybrid AUV/ROV system," in *Proc. Int. Symp. Underwater Technol.*, Apr. 19, 2002, pp. 17–23.
[36] N. Tito and E. Rambaldi, "SWIMMER: Innovative IMR AUV," in *Proc. Offshore Technol. Conf.*, Houston, TX, USA, May 4–7, 2009.
[37] P. Ridao, M. Carreras, D. Ribas, P. Sanz, and G. Oliver, "Intervention AUVs: The next challenge," in *Proc. 19th IFAC World Congr.*, Cape Town, South Africa, Aug. 24–29, 2014, pp. 12 146–12 159.
[38] J. Evans, P. Redmond, C. Plakas, K. Hamilton, and D. Lane, "Autonomous docking for intervention-AUVs using sonar and video-based real-time 3d pose estimation," in *Proc. MTS/IEEE OCEANS*, 2003, pp. 2201–2210.
[39] G. Marani, S. K. Choi, and J. Yuh, "Underwater autonomous manipulation for intervention missions AUVs," *Ocean Eng.*, vol. 36, no. 1, pp. 15–23, 2009.
[40] D. Ribas, N. Palomeras, P. Ridao, M. Carreras, and A. Mallios, "Girona 500 AUV: From survey to intervention," *IEEE/ASME Trans. Mechatronics*, vol. 17, no. 1, pp. 46–53, Feb. 2012.
[41] M. Prats *et al.*, "Reconfigurable AUV for intervention missions: a case study on underwater object recovery," *Intell. Service Robot.*, vol. 5, no. 1, pp. 19–31, 2012.
[42] P. J. Sanz *et al.*, "TRIDENT: A framework for autonomous underwater intervention missions with dexterous manipulation capabilities," *IFAC Proc. Vol.*, vol. 43, no. 16, pp. 187–192, 2010.
[43] L. Brignone, E. Raugel, J. Opderbecke, V. Rigaud, R. Piasco, and S. Ragot, "First sea trials of HROV the new hybrid vehicle developed by IFREMER," in *Proc. MTS/IEEE OCEANS*, Genova, Italy, May 18–21, 2015, pp. 1–7.
[44] H-ROV Ariane. ECA Group and Ifremer, 2017. [Online]. Available: http://www.ecagroup.com/en/solutions/h-rov
[45] Y. Nakamura, H. Hanafusa, and T. Yoshikawa, "Task-priority based redundancy control of robot manipulators," *Int. J. Robot. Res.*, vol. 6, no. 2, pp. 3–15, 1987.
[46] G. Antonelli, "A new adaptive control law for the phantom ROV," *IFAC Proc. Vol.*, vol. 36, no. 17, pp. 479–484, 2003.
[47] G. Antonelli, F. Caccavale, S. Chiaverini, and G. Fusco, "A novel adaptive control law for underwater vehicles," *IEEE Trans. Control Syst. Technol.*, vol. 11, no. 2, pp. 221–232, Mar. 2003.
[48] G. Antonelli, F. Caccavale, and S. Chiaverini, "A virtual decomposition based approach to adaptive control of underwater vehicle-manipulator systems," in *Proc. 9th IEEE Mediterranean Conf. Control Autom.*, Dubrovnik, Croatia, Jun. 2001, pp. 1–5.
[49] G. Antonelli, F. Caccavale, and S. Chiaverini, "Adaptive tracking control of underwater vehicle-manipulator systems based on the virtual decomposition approach," *IEEE Trans. Robot. Autom.*, vol. 20, no. 3, pp. 594–602, Jun. 2004.
[50] B. Lynch and A. Ellery, "Efficient control of an AUV-manipulator system: An application for the exploration of Europa," *IEEE J. Ocean. Eng.*, vol. 39, no. 3, pp. 552–570, Jul. 2014.
[51] A. Sans-Muntadas, E. Kelasidi, K. Pettersen, and E. Brekke, "Spiral path planning for docking of underactuated vehicles with limited FOV," in *Proc. 1st IEEE Conf. Control Technol. Appl.*, Mauna Lani, HI, USA, Aug. 27–30, 2017, pp. 732–739.
[52] K. Y. Pettersen and E. Lefeber, "Way-point tracking control of ships," in *Proc. 40th IEEE Conf. Decision Control*, 2001, pp. 940–945.
[53] T. I. Fossen, M. Breivik, and R. Skjetne, "Line-of-sight path following of underactuated marine craft," *IFAC Proc. Vol.*, vol. 36, no. 21, pp. 211–216, 2003.
[54] E. Kelasidi, K. Y. Pettersen, and J. T. Gravdahl, "A waypoint guidance strategy for underwater snake robots," in *Proc. IEEE 22nd Mediterranean Conf. Control Autom.*, Palermo, Italy, Jun. 16–19, 2014, pp. 1512–1519.
[55] I. Schjølberg and T. Fossen, "Modelling and control of underwater vehicle-manipulator systems," in *Proc. 3rd Conf. Marine Craft Maneuv. Control*, Southampton, U.K., Sep. 1994, pp. 45–57.
[56] S. F. Hoerner, *Fluid Dynamic Drag: Practical Information on Aerodynamic Drag and Hydrodynamic Resistance*. Bricktown, NJ, USA: Hoerner Fluid Dynamics, 1965.

Jørgen Sverdrup-Thygeson received the M.Sc. degree in engineering cybernetics from Norwegian University of Science and Technology (NTNU), Trondheim, Norway, in 2007. He is currently working toward the Ph.D. degree (VISTA Scholar) at the CoE Centre for Autonomous Marine Operations and Systems, Department of Engineering Cybernetics, NTNU.

In 2007–2015, he was with the companies Marine Cybernetics AS and Kongsberg Oil and Gas Technologies. His current research interests include modeling, simulation, and control of underwater snake robots equipped with thrusters.

Eleni Kelasidi received the M.Sc. degree in electrical and computer engineering from the University of Patras, Patras, Greece, in 2009, and the Ph.D. degree in engineering cybernetics from Norwegian University of Science and Technology (NTNU), Trondheim, Norway, in 2015.

During 2009–2012, she was a Predoctoral Researcher in the field of design and control of mobile robot with articulated body at the University of Patras. She is currently a Postdoctoral Researcher (VISTA Scholar) at the CoE Centre for Autonomous Marine Operations and Systems, Department of Engineering Cybernetics, NTNU. Her research interests include modeling, analysis, and control of underwater snake robots.

Kristin Y. Pettersen (F'17) received the M.Sc. and Ph.D. degrees in engineering cybernetics from Norwegian University of Science and Technology (NTNU), Trondheim, Norway, in 1992 and 1996, respectively.

She is currently a Professor in the Department of Engineering Cybernetics, NTNU, where she has been a faculty member since 1996. She was the Head of the department during 2011–2013, Vice Head of the department during 2009–2011, and the Director of the NTNU ICT Programme of Robotics during 2010–2013. She is an Adjunct Professor at the Norwegian Defence Research Establishment. For the period 2013–2022, she is also the Key Scientist at the CoE Centre for Autonomous Marine Operations and Systems. She is a cofounder of the NTNU spin-off company Eelume AS, where she was the CEO during 2015–2016. She has authored/co-authored more than 200 papers in scientific conferences and journals, and her research interests focus on nonlinear control of mechanical systems with applications to robotics, with a special emphasis on marine robotics and snake robotics.

Dr. Pettersen and her co-authors received the IEEE TRANSACTIONS ON CONTROL SYSTEMS AND TECHNOLOGY Outstanding Paper Award for "Global uniform asymptotic stabilization of an underactuated surface vessel: Experimental results." She is a member of the IFAC Council and was a member of the Board of Governors of the IEEE Control Systems Society 2012–2014. She has also held several board positions in industrial and research companies. She is a member of the Norwegian Academy of Technological Sciences.

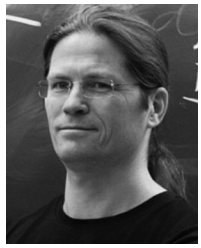

Jan Tommy Gravdahl received the Siv. Ing and Dr. Ing degrees in engineering cybernetics from Norwegian University of Science and Technology (NTNU), Trondheim, Norway, in 1994 and 1998, respectively.

He was appointed as an Associate Professor in 2001 and a Professor in 2005 in the Department of Engineering Cybernetics, NTNU, where he also served as the Head of the department in 2008–2009. During 2007–2008, he was a Visiting Professor at The Centre for Complex Dynamic Systems and Control (CDSC), The University of Newcastle, Callaghan NSW, Australia. He has authored/co-authored 5 books and more than 200 papers in international conferences and journals. His current research interests include mathematical modeling and nonlinear control in general, modeling and control of turbomachinery, and control of vehicles, spacecraft, robots, and high-precision mechatronic systems.

Dr. Gravdahl received the IEEE TRANSACTIONS ON CONTROL SYSTEMS AND TECHNOLOGY Outstanding Paper Award for the paper "Centrifugal compressor surge and speed Control." He is a Senior Editor of the IFAC journal *Mechatronics*.